Neurobiology of Disease 143 (2020) 104994

Contents lists available at ScienceDirect

Neurobiology of Disease

journal homepage: www.elsevier.com/locate/ynbdi

Effects of EHP-101 on inflammation and remyelination in murine models of Multiple sclerosis

Carmen Navarrete[a], Adela García-Martin[b], Martín Garrido-Rodríguez[c,d,e], Leyre Mestre[f], Ana Feliú[f], Carmen Guaza[f], Marco A. Calzado[c,d,e], Eduardo Muñoz[c,d,e,*]

[a] Emerald Health Pharmaceuticals, San Diego, CA, USA
[b] Emerald Health Biotechnology, Córdoba, Spain
[c] Instituto Maimónides de Investigación Biomédica de Córdoba, Spain
[d] Departamento de Biología Celular, Fisiología e Inmunología, Universidad de Córdoba, Spain
[e] Hospital Universitario Reina Sofía, Córdoba, Spain
[f] Departamento de Neurobiología Funcional y de Sistemas, Instituto Cajal-CSIC, Madrid, Spain

ARTICLE INFO

Keywords:
Multiple sclerosis
EHP-101
Transcriptomic
Inflammation
Remyelination

ABSTRACT

Multiple Sclerosis (MS) is characterized by a combination of inflammatory and neurodegenerative processes in the spinal cord and the brain. Natural and synthetic cannabinoids such as VCE-004.8 have been studied in preclinical models of MS and represent promising candidates for drug development. VCE-004.8 is a multitarget synthetic cannabidiol (CBD) derivative acting as a dual Peroxisome proliferator-activated receptor-gamma/Cannabinoid receptor type 2 (PPARγ/CB_2) ligand agonist that also activates the Hypoxia-inducible factor (HIF) pathway. EHP-101 is an oral lipidic formulation of VCE-004.8 that has shown efficacy in several preclinical models of autoimmune, inflammatory, fibrotic, and neurodegenerative diseases. EHP-101 alleviated clinical symptomatology in EAE and transcriptomic analysis demonstrated that EHP-101 prevented the expression of many inflammatory genes closely associated with MS pathophysiology in the spinal cord. EHP-101 normalized the expression of several genes associated with oligodendrocyte function such as Teneurin 4 (Tenm4) and Gap junction gamma-3 (Gjc3) that were downregulated in EAE. EHP-101 treatment prevented microglia activation and demyelination in both the spinal cord and the brain. Moreover, EAE was associated with a loss in the expression of Oligodendrocyte transcription factor 2 (Olig2) in the corpus callosum, a marker for oligodendrocyte differentiation, which was restored by EHP-101 treatment. In addition, EHP-101 enhanced the expression of glutathione S-transferase pi (GSTpi), a marker for mature oligodendrocytes in the brain. We also found that a diet containing 0.2% cuprizone for six weeks induced a clear loss of myelin in the brain measured by Cryomyelin staining and Myelin basic protein (MBP) expression. Moreover, EHP-101 also prevented cuprizone-induced microglial activation, astrogliosis and reduced axonal damage. Our results provide evidence that EHP-101 showed potent anti-inflammatory activity, prevented demyelination, and enhanced remyelination. Therefore, EHP-101 represents a promising drug candidate for the potential treatment of different forms of MS.

Abbreviations: BBB, Blood-brain-barrier; CB2, Cannabinoid receptor type 2; CBD, Cannabidiol; Ccl2, C-C Motif Chemokine Ligand 2; Ccl4, C-C Motif Chemokine Ligand 4; CNS, Central nervous system; CPZ, Cuprizone; EAE, Experimental autoimmune encephalomyelitis; ECS, Endocannabinoid system; EPO, Erythropoietin; FGF-2, Fibroblast growth factor; GFAP, Glial fibrillary acidic protein; Gjc3, Gap junction gamma 3; GO, Gene Ontology; GSTpi, Glutathione S-transferase pi; HIF, Hypoxia-inducible factor; Iba-1, Ionized calcium binding adaptor molecule 1; IGF-1, Insulin-like growth factor; IHC, Immunohistochemistry; Il1b, Interleukin 1 beta; Il6, Interleukin 6; MBP, Myelin basic protein; MOG35–55, Myelin Oligodendrocyte Glycoprotein Peptide Fragment 35–55; MS, Multiple Sclerosis; Olig2, Oligodendrocyte transcription factor 2; OPC, Oligodendrocyte progenitor cell; PDGF-α, Platelet-derived growth factor alpha; PPARɣ, Peroxisome proliferator-activated receptor-gamma; PHDs, Prolyl hydroxylases; RRMS, Relapsing-remitting MS; SMI-32, mouse anti-Neurofilament H (NF-H) Nonphosphorylated antibody; Tenm4, Teneurin 4; Timp1, Tissue inhibitor matrix metalloproteinase 1; TRP channels, Transient receptor potential channels; Vcam, Vascular cell adhesion molecule 1

* Corresponding author at: Maimónides Biomedical Research Institute of Córdoba, University of Córdoba, Avda Menéndez Pidal s/n, 14004 Córdoba, Spain.
E-mail address: fi1muble@uco.es (E. Muñoz).

https://doi.org/10.1016/j.nbd.2020.104994
Received 27 March 2020; Received in revised form 5 June 2020; Accepted 20 June 2020
Available online 26 June 2020

1. Introduction

Multiple sclerosis (MS) is an autoimmune disease that affects the central nervous system (CNS) and is characterized by pathological changes, including neuroinflammation, demyelination and axon injury (Kipp et al., 2009; Lassmann, 2010; Scolding and Franklin, 1998). The spontaneous repair of damaged myelin sheaths and axons has been described during the remission period of classical relapsing-remitting MS (RRMS), where demyelinated axons could be rewrapped by the regenerated myelin sheath, thus ameliorating axonal dysfunction. In this sense, the remission period is also considered the period of remyelination (Fox et al., 2015; Kister et al., 2013), which is important because it could be a key time for the treatment of RRMS patients with drugs preventing inflammation and enhancing remyelination.

Small molecules including cannabinoids acting at druggable targets of the endocannabinoid system (ECS) are being explored for the management of CNS pathologies including MS (Chiurchiu et al., 2018). In this sense, several lines of evidence suggested a role for the ECS in oligodendrocyte function and remyelination activity in MS (Bernal-Chico et al., 2015; Feliu et al., 2017; Ilyasov et al., 2018). The ECS is composed by the G-protein coupled receptors Cannabinoid type 1 (CB_1) and type 2 (CB_2), endocannabinoids and the enzymes regulating their synthesis and catabolism. In addition, cannabinoids of a different nature also target ionotropic receptors of the Transient receptor potential channels (TRP channels) family and nuclear receptors such as peroxisome proliferator-activated receptors (PPARs) (Barrie and Manolios, 2017; Pistis and O'Sullivan, 2017). CB_1 receptors are expressed mainly in the CNS at neuronal terminals and regulate neurotransmitter release and psychoactive processes. In contrast, CB_2 receptors are located primarily in the peripheral immune system, and its expression is increased during neuroinflammation on activated microglia in the CNS (Pacher and Mechoulam, 2011; Sanchez and Garcia-Merino, 2012). Key considerations for developing CB_2 receptor agonists include absence of psychoactive effects, sustained anti-inflammatory activity, tissue/cell protection, lack of cardiovascular adverse effects and efficacy in several disease models on neuroinflammation including MS (Kong et al., 2014; Navarrete et al., 2018; Pacher and Kunos, 2013; Pacher and Mechoulam, 2011; Tomas-Roig et al., 2016).

PPARs are members of the nuclear hormone receptor superfamily of ligand-activated transcriptional factors (Ricote et al., 1998a) with well-identified regulatory roles in lipid and glucose homeostasis and adipocyte differentiation (Straus and Glass, 2007). In addition to adipocytes and hepatocytes, PPARγ has been shown to be expressed in different CNS cells and in immune cells (Bernardo and Minghetti, 2006). Furthermore, PPARγ has been described as an important factor in the regulation of the immune response (Daynes and Jones, 2002). In this sense, PPARγ activation has been shown to suppress the expression of inflammatory cytokines in astrocytes and macrophages/microglia (Ricote et al., 1998b; Storer et al., 2005; Xu et al., 2007). Furthermore, PPARγ stimulated oligodendrocyte differentiation from neural stem cells (Kanakasabai et al., 2012), promoted and accelerated the differentiation of oligodendrocyte progenitor cells in vitro with an additional increase in antioxidant defences (Bernardo et al., 2009; De Nuccio et al., 2011) and increased lipid production and terminal differentiation of cultured oligodendrocytes (Roth et al., 2003), thus suggesting an additional possible protective role of PPARγ in MS as a mediator of remyelination. The neuroprotective effects of PPARs, including PPARγ, have also been widely documented in vitro in various experimental paradigms of neurodegeneration, broadening its potential therapeutic perspectives in MS (Brodbeck et al., 2008; Inestrosa et al., 2005; Luna-Medina et al., 2005; Zhao et al., 2006).

We have previously shown that VCE-004.8 is a promising cannabidiol (CBD) derivative acting as a dual agonist of PPARγ and CB_2 that also activates the HIF pathway (Navarrete et al., 2018). Indeed, VCE-004.8 prevented neuroinflammation and demyelination in two different murine models of MS, namely EAE and Theiler's virus-induced demyelinating disease (Navarrete et al., 2018). EHP-101 is an oral formulation of VCE-004.8 that also showed efficacy in a murine model of systemic sclerosis (SSc) (Garcia-Martin et al., 2019; Garcia-Martin et al., 2018). EHP-101 has completed a Phase I clinical study (clinicaltrial.gov: NCT03745001) and initiation of Phase II studies in SSc and MS patients are being planned.

Although most current therapies for MS are directed towards modulation of the exacerbated immune response (McFarland and Martin, 2007), novel therapies aimed at axonal remyelination are urgently needed. Herein we show the efficacy of EHP-101 in preventing neuroinflammation and demyelination in EAE and enhancing remyelination in the cuprizone model of demyelination.

2. Material and methods

2.1. Compounds

For preparing EHP-101, VCE-004.8 [(1′*R*,6′*R*)-3-(Benzylamine)-6-hydroxy-3′-methyl-4-pentyl-6′-(prop-1-en-2-yl) [1,1'bi(cyclohexane)]-2′,3,6-triene-2,5-dione)] was dissolved in Corn oil and Maisine® CC (1:1) (Garcia-Martin et al., 2018). The chromatographic purity of VCE-004.8 in EHP-101 was 97.6%.

2.2. Animals

All experiments were performed in strict accordance with European Union (EU) and governmental regulations. Handling of animals was performed in compliance with the guidelines of animal care set by the EU guidelines 86/609/EEC, and the Ethics Committees on Animal Experimentation at the Cajal Institute (CSIC, Madrid) and the University of Córdoba (UCO, Córdoba, Spain) approved all the procedures described in this study (for EAE at Cajal Institute protocol number: 96 2013/03 CEEA-IC and for cuprizone model at UCO protocol number: 2018PI/02 (UCO). Measures to improve welfare assistance and clinical status as well as endpoint criteria were established to minimize suffering and ensure animal welfare. Briefly, wet food pellets are placed on the bed-cage when the animals begin to develop clinical signs to facilitate access to food and hydration. For the EAE model, female C57BL/6 mice were purchased from Harlan (Barcelona, Spain) and for the cuprizone model, male C56BL/6 mice were purchased from Janvier Labs (Le Genest-Saint-Isle, France). All animals were housed in the animal facilities under the following controlled conditions: 12 h light/dark cycle; temperature 20 °C (± 2 °C) and 40–50% relative humidity with free access to standard food and water.

2.3. Induction and assessment of EAE

EAE was induced in C57BL/6 female mice at 6–8 weeks of age by subcutaneous immunization with Myelin Oligodendrocyte Glycoprotein Peptide Fragment 35–55 (MOG35–55) (300 μg: peptide synthesis section, CBM, CSIC, Madrid, Spain) and 200 μg of *Mycobacterium tuberculosis* (H37Ra Difco, Franklin Lakes, NJ, USA) in a 1:1 mix with incomplete Freund's adjuvant (CFA, Sigma). On the same day and 2 days later, mice were injected intraperitoneally with 200 ng of pertussis toxin (Sigma) in 0.1 ml Phosphate buffer saline (PBS). Control animals (CFA) were inoculated with the same emulsion without MOG and they did not receive pertussis toxin. Treatment started at day 8 post-immunization when animals showed the first symptoms of the disease and consisted of daily oral EHP-101 administration (1, 5, 10 and 20 mg/kg) for the following 21 days. The mice were examined daily for clinical signs of EAE and disease scores were measured as follows: 0, no disease; 1, limb tail; 2, limb tail and hind limb weakness; 3, hind limb paralysis; 4, hind limb and front limb paralysis; 5, moribund and death. All animals were sacrificed at 28 days for further analysis.

2.4. Cuprizone-induced demyelination

To induce demyelination, 8-week old C57BL/6 male mice were fed with 0.2% cuprizone (CPZ) TD.140800 diet (Envigo, Barcelona, Spain) for six weeks. Control group (no demyelination) was fed with control mouse TD.00217 diet (Envigo, Barcelona, Spain) for the entire period. To study the effect on remyelination, EHP-101 was administered once daily by oral gavage at 20 mg/kg from week six. For comparison, animals in the CPZ control group (maximal demyelination) received the same volume of vehicle by gavage. To study the dynamic effect of EHP-101 on remyelination, animals in each group were sacrificed at weeks 6, 7 (6 + 1 W), 8 (6 + 2 W) for further analysis.

2.5. Tissue processing

Mice were anesthetized by i.p. administration of a ketamine-xylazine or pentobarbital solution and they were transcardially perfused with saline 0.9%. The spinal cord was obtained by extrusion with saline. Brain and cervical spinal cord were immediately frozen and kept at −80 °C for RT-PCR analysis. The remaining brain and spinal cord were fixed in 4% paraformaldehyde in 0.1 M PBS, washed in 0.1 M PBS, cryoprotected with a 15% and then a 30% solution of sucrose in 0.1 M PBS, and frozen at −80 °C. Free-floating brain (sections were taken between bregma 0.38 and 0.98 mm) and thoracic spinal cord sections (50 μm thick: Leica Microsystems CM1900 cryostat, Barcelona, Spain) were then processed for immunohistochemistry or immunofluorescence. In the case of cuprizone model whole brains were fixed, cryoprotected and frozen at −80 °C for further analysis.

2.6. Inflammatory infiltrate analysis

Spinal cord slices were stained with hematoxylin-eosin (H&E) to analyze the infiltrates in the parenchyma. Inflammatory infiltrates were evaluated on a scale of 0 to 4, the score reflecting the number of infiltrates in the thoracic spinal cord sections. A score of 4 reflects the largest number of infiltrates with all the intermediate scores (1, 2, and 3) defining the increase in the density of infiltrates in the spinal cord tissue.

2.7. Immunohistochemical analysis

For IHC analysis, free-floating thoracic spinal cord (50 μm) sections were washed with 0.1 M Phosphate buffer (PB). Endogenous peroxidase activity was inhibited with 3.3% hydrogen peroxide in methanol. The sections were blocked with 2.5% normal horse serum and then incubated overnight at 4 °C in blocking buffer with a rabbit anti-Teneurin 4 antibody (1:50: Novus Biological, Colorado, USA) or anti-CD3 antibody (1:50: Santa Cruz Biotechnology, Santa Cruz, CA, USA). Slides were incubated with ImmPRESS reagent (Vector Laboratories; Burlingame, Ca, USA) and then developed with diaminobenzidine chromogen (Merck, Darmstadt, Germany). Samples were photographed, digitalized using a Leica DFC420c camera and analyzed using Image J software. Myelin integrity was analyzed using the Hito CryoMyelinStain™ Kit (Gold phosphate complex Myelin Staining Kit) following manufacturer's recommendation (Hitobiotech Corp., Kingsport, TN, USA).

2.8. Confocal microscopy analysis

For antigen retrieval, spinal cord or brain sections were boiled for 10 min in sodium citrate buffer (10 mM, pH 6.0) or Tris-EDTA buffer (10 mM Tris Base, 1 mM EDTA, 0.05% Tween 20, pH 9.0) (Sigma-Aldrich, St. Louis, MO, USA). The sections were washed three times in PBS. Nonspecific antibody-binding sites were blocked for 1 h at room temperature with 3% bovine serum albumin (BSA) (Sigma-Aldrich, St. Louis, MO, USA in PBS). Next, the sections were incubated overnight at 4 °C with the following primary antibodies diluted in PBS with 3% BSA: microglia cells were stained with a rabbit anti-ionized calcium binding adaptor molecule 1 (Iba-1) antibody (1:1,000; Wako Chemical Pure Industry, Osaka, Japan), astrocytes were stained with a mouse anti-glial fibrillary acidic protein (GFAP) antibody (1:500, Santa Cruz Biotechnology, Santa Cruz, CA, USA), myelin basic protein was marked with a rabbit anti-Myelin Basic Protein (MBP) antibody (1:1000; Abcam, Cambridge, UK), oligodendrocytes were marked with a mouse anti-Olig2 (1:100, Santa Cruz, CA, USA) and a rabbit anti-GSTPi (1:250, Abcam, Cambridge, UK) axonal damage was determined with a mouse anti-Neurofilament H (NF-H) Nonphosphorylated antibody (SMI-32) (1:50; Biolegend, CA, USA). After extensive washing in PBS, slides were incubated with secondary antibodies for 1 h at room temperature in the dark. The immunoreactions were revealed using anti-rabbit Texas Red (1:100), anti-mouse/rabbit Alexa 488 (1:100) obtained from Thermo Fischer Scientific, Walthamm, MA, USA. The slides were then mounted using Vectashield Antifade Mounting Medium with DAPI (Vector Laboratories, Burlingame, Ca, USA). All images were acquired using a spectral confocal laser-scanning microscope LSM710, (Zeiss, Jena, Germany) with a 20×/0.8 Plan-Apochromat lens and quantified in 9–15 randomly chosen fields using ImageJ software (http://rsbweb.nih.gov/ij/).

2.9. RNA-Seq and bioinformatic analysis

Total RNA was isolated from spinal cord tissue using QIAzol lysis reagent (Qiagen, Hilden, Germany) and purified with RNeasy Lipid Tissue Mini kit (Qiagen). Then, samples were processed for high throughput sequencing using poly-A selection with the TruSeq Stranded mRNA Library Prep Kit (Cat. No. RS-122-2101, Illumina, San Diego, CA, USA). In brief, 1 μg of total RNA from each sample was used to construct a cDNA library, followed by sequencing on the Illumina HiSeq 2500 system with single end 50 bp reads and ~ 40 millions of reads per sample (n = 3 per group). FASTQ files were pre-processed with Trimmomatic (v0.36) (Bolger et al., 2014) and aligned to mouse genome assembly mm10 using HISAT2 (v2.1.0) (Kim et al., 2015). Then, counts per gene matrix were obtained with featureCounts (v1.6.1) (Liao et al., 2014) using the in-built RefSeq annotation for mm10 genome assembly and the differential expression analysis was carried out using DESeq2 (v1.20.0) (Love et al., 2014), excluding genes with less than 15 counts across all samples. The functional over-representation analyses were performed using EnrichR (Kuleshov et al., 2016) and clusterProfiler (Yu et al., 2012). All the P values were adjusted to control the false discovery rate (FDR) using the Benjamini and Hochberg approach (Klipper-Aurbach et al., 1995). RNA-seq data have been deposited in the Gene Expression Omnibus databank (accession no. GSE131854).

2.10. Quantitative reverse transcriptase-PCR

Total RNA (1 μg) was retrotranscribed using the iScript cDNA Synthesis Kit (Bio-Rad, Hercules, CA, USA) and the cDNA analyzed by real-time PCR using the iQTM SYBR Green Supermix (Bio-Rad) and a CFX96 Real-time PCR Detection System (Bio-Rad). Glyceraldehyde-3-Phosphate Dehydrogenase (GAPDH) gene was used to standardize mRNA expression in each sample. Gene expression was quantified using the 2-ΔΔCt method and the percentage of relative expression against controls was represented. The primers used in this study are described in Table A.1.

2.11. Data analysis

All the in vivo data are expressed as the mean ± SEM. One-way analysis of variance (ANOVA) followed by the Tukey's post-hoc test for parametric analysis or Kruskal-Wallis post-hoc test in the case of non-parametric analysis tests were used to determine the statistical

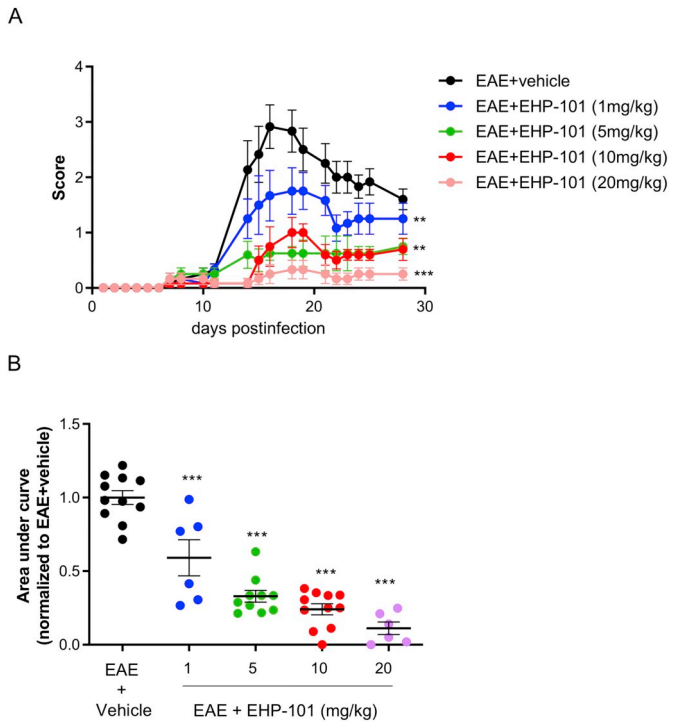

Fig. 1. EHP-101 attenuates clinical severity and neuropathology in EAE model. (**A**) EHP-101 significantly ameliorated the clinical signs and progression of EAE. Results are expressed as mean ± SEM (n = 6 animals per group). $^{**}p < .01$, $^{***}p < .001$ EAE + EHP-101 vs EAE + Vehicle (one-way ANOVA followed by the Tukey's post-hoc test). **(B)** Clinical activity was quantified by measuring the area under curve. Results are expressed as mean ± SEM (n = 6 animals per group). $^{***}p < .001$ EAE + EHP-101 vs EAE + Vehicle (one-way ANOVA followed by the Tukey's post-hoc test).

significance. The level of significance was set at $p^{<}0.05$. Statistical analyses were performed using GraphPad Prism version 8.00 (GraphPad, San Diego, CA, USA).

3. Results

3.1. EHP-101 attenuates clinical severity and neuroinflammation in EAE

The efficacy of EHP-101 in MS was first evaluated in EAE, performing the treatments at an early stage of the disease since mice received increasing doses of EHP-101 at day 8 post-immunization (p.i.). Subcutaneous immunization with MOG35–55 induced EAE in all mice that received the vehicle alone. All vehicle-treated mice developed a disease that peaked by day 16 p.i. and maintained at day 28 p.i. By contrast, the reduced clinical score showed therapeutic efficacy of EHP-101 with all the dose levels tested, with the highest dose (20 mg/kg) able to prevent the symptoms completely (Fig. 1A $p = .0002$ EAE + EHP-101 20 mg/kg vs EAE + Vehicle; $p = .0046$ EAE + EHP-101 10 mg/kg vs EAE + Vehicle; $p = .0068$ EAE + EHP-101 5 mg/kg vs EAE + Vehicle). Clinical score data from Fig. 1 used to determine the area under curve as shown in Fig. 1B ($p < 0.0001$ EAE + EHP-101 1/5/10/20 mg/kg vs EAE + Vehicle) clearly demonstrated that EHP-101 improved symptomatology in a dose-dependent manner.

To determine whether EHP-101 was able to target neuroinflammation in EAE, immune cell infiltration, microgliosis and astrogliosis were evaluated in the spinal cord. Histopathological analysis showed that infiltration of immune cells into the spinal cord was reduced by EHP-101 treatment as shown by hematoxylin-eosin staining (Fig. 2A, B $p < 0.0001$ EAE + Vehicle vs CFA; $p = .0015$ EAE + EHP-101 20 mg/kg vs EAE + Vehicle). In addition, EHP-101 treatment reduced the number of $CD3^+$ T cells in the spinal cord of EAE mice (Fig. 2A, C $p < 0.0001$ EAE + Vehicle vs CFA; $p = .0456$ EAE + EHP-101 20 mg/kg vs EAE + Vehicle). Moreover the extensive microglia/macrophage activation (Fig. 2A, D $p = .0003$ EAE + Vehicle vs CFA; $p = .0006$ EAE + EHP-101 20 mg/kg vs EAE + Vehicle) and astrocyte activation (Fig. 2A, E $p < 0.0001$ EAE + Vehicle vs CFA; $p = .0051$ EAE + EHP-101 20 mg/kg vs EAE + Vehicle) in the spinal cord of EAE mice evidenced by both Iba-1 and GFAP staining was greatly reduced by EHP-101.

MS pathology is characterized by focal demyelinating lesions in the CNS at both spinal cord and brain levels. Therefore, to determine the extent of demyelination, myelin was evaluated by MBP immunolabelling. A clear demyelination was found in the spinal cord of EAE mice that was significantly prevented by EHP-101 treatment (Fig. 2A, F $p = .0001$ EAE + Vehicle vs CFA; $p < 0.0001$ EAE + EHP-101 vs EAE + Vehicle).

Cerebral cortical demyelination as well as callosal pathology are widely recognized features of MS (Kornek and Lassmann, 2003; Rasmussen et al., 2007; Storch et al., 2006). In addition, the cerebral cortex plays a central role in interhemispheric communication, and callosal atrophy in MS patients has been shown to correlate with disability status (Bonzano et al., 2008; Manson et al., 2006; Manson et al., 2008). Therefore, we also examined whether these structures might also be affected in EAE mice. An increase in inflammatory lesions was seen throughout the EAE forebrain (Fig. 3A). Specifically, we observed that microglial reactivity was increased in corpus callosum of EAE mice and the treatment with EHP-101 reverted the microgliosis process (Fig. 3B $p = .0002$ EAE + Vehicle vs CFA; $p = .0395$ EAE + EHP-101 20 mg/kg vs EAE + Vehicle). Furthermore, brain sections from EAE-affected mice were also analyzed for the distribution of MBP reactivity. MBP immunoreactivity appeared significantly reduced in cerebral cortex (Fig. 3C $p = .0159$ EAE + Vehicle vs CFA; $p = .0024$ EAE + EHP-101 20 mg/kg vs EAE + Vehicle) and this loss of myelin expression was strongly reverted by EHP-101 treatment. Moreover, EAE is associated with a loss in the expression of Olig2 in the corpus callosum, a marker for the onset of oligodendrocyte differentiation, which was restored by EHP-101 treatment (Fig. 3D $p < 0.0001$ EAE + Vehicle vs CFA; $p = .0008$ EAE + EHP-101 20 mg/kg vs EAE + Vehicle). In addition, EHP-101 enhanced the expression of glutathione S-transferase pi (GSTpi), a cytosolic isoenzyme used as a marker for mature oligodendrocytes in the brain (Fig. 3E $p = .0222$ EAE + EHP-101 20 mg vs EAE + Vehicle). These data are indicative of the potential of EHP-101 to prevent demyelination in an MS murine model.

3.2. EHP-101 normalizes EAE transcriptomic signature in the spinal cord

To evaluate the global expression changes produced by EHP-101 treatment, we performed an RNA-Seq analysis of the spinal cords from mice in the following conditions: Control, EAE and EAE with EHP-101 treatment (20 mg/kg). Sequencing data for three biological replicates were obtained for each experimental group. Then, we compared the transcriptomic profile between the different conditions to get a first insight into the changes occurring in the model, with or without treatment. As expected, we found many changes, both in magnitude and significance in EAE mice compared to the group treated with EHP-101 (Fig. 4A). Then, to evaluate those changes at a biological level, we performed an over-representation analysis using genes that surpassed the cutoff of an adjusted $P < .05$ and absolute fold change > 2 in the EAE vs control and EAE + EHP-101 vs EAE comparisons. The more significant enrichments were found in the groups of upregulated genes by EAE and downregulated genes by the treatment. We observed a complementary signature between those two groups, where gene ontology terms like “regulation of immune response”, “inflammatory response” or “cytokine-mediated signaling pathway” appeared, highlighting an anti-inflammatory effect of the EHP-101 treatment on the spinal cord. Interestingly, among those genes participating in the inflammatory response, we also found enriched terms related with the

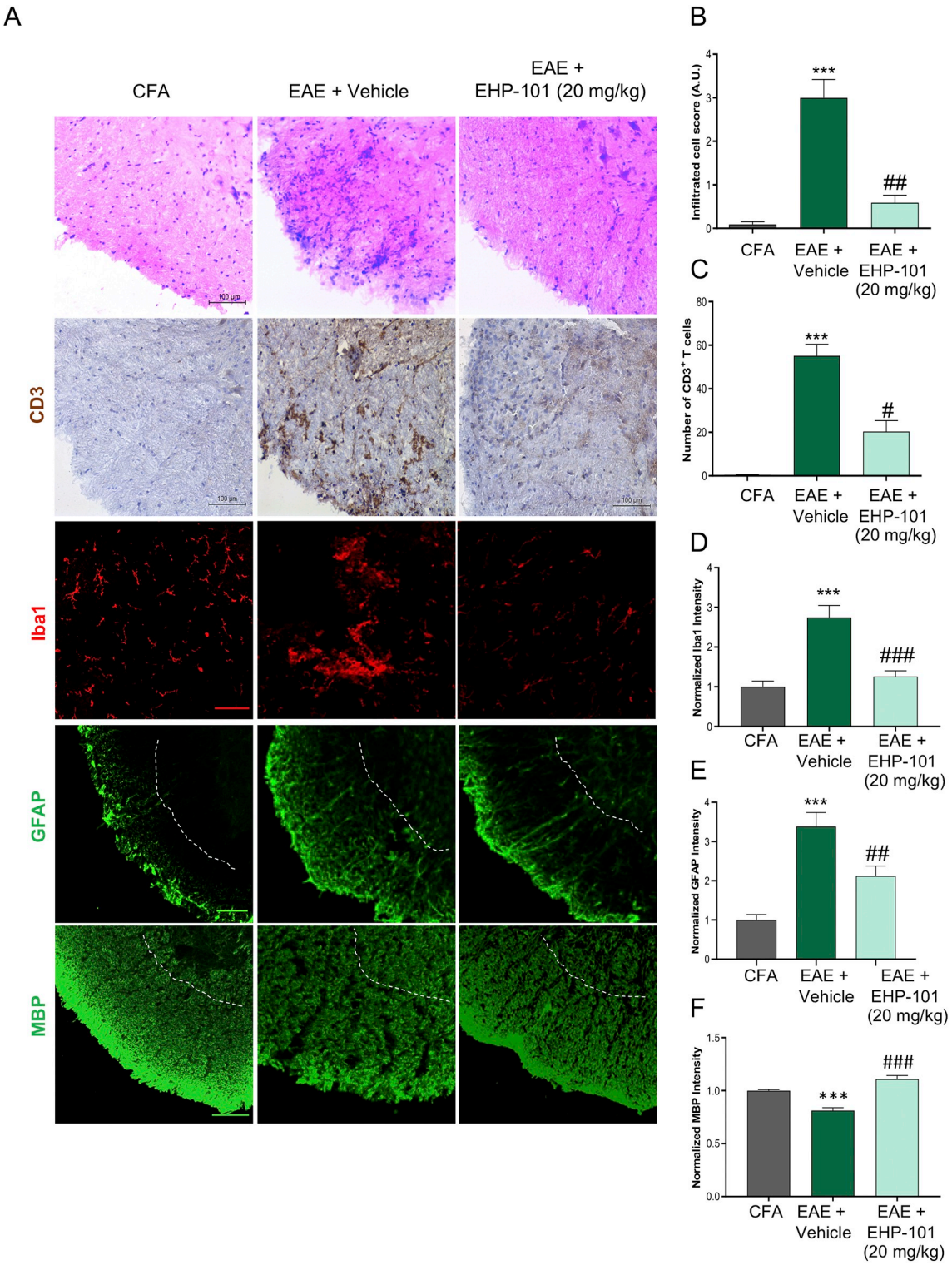

Fig. 2. EHP-101 significantly reduces glial reactivity and preserves myelin structure in the spinal cord of EAE animals. (**A**) Cross-sectional images of thoracic spinal cord of 50 µm thick, in which hematoxylin-eosin staining, immunohistochemistry with anti-CD3 and immunofluorescence with anti-Iba1, GFAP and myelin staining MBP were studied in the white matter (dashed line separates gray and white matter). Scale bars equivalent to 100 µm. The quantifications of each marker (**B**–**F**) are shown as mean ± SEM (n = 5 animals per group), and significance was determined by one-way ANOVA followed by the Tukey's or Kruskall-Wallis post-hoc tests. ***p < .001 EAE + Vehicle vs CFA; #p < .05, ##p < .01, ###p < .001 EAE + EHP-101 vs EAE + Vehicle.

cellular response to oxidative stress as "cellular response to oxygen-containing compound", "positive regulation of reactive oxygen species biosynthetic process" or "positive regulation of superoxide anion generation" (Fig. 4B). The heatmap in Fig. 4C represents genes from the "cytokine-mediated signaling pathway" that are induced by EAE and downregulated by EHP-101. Furthermore, to confirm this anti-inflammatory effect of EHP-101 in the spinal cord we determined the gene expression by RT-PCR of several genes such as Interleukin 6 (IL-6), Tissue inhibitor matrix metalloproteinase 1 (Timp1), vascular cell adhesion molecule 1 (Vcam), Interleukin 1 beta (IL-1β), C–C Motif

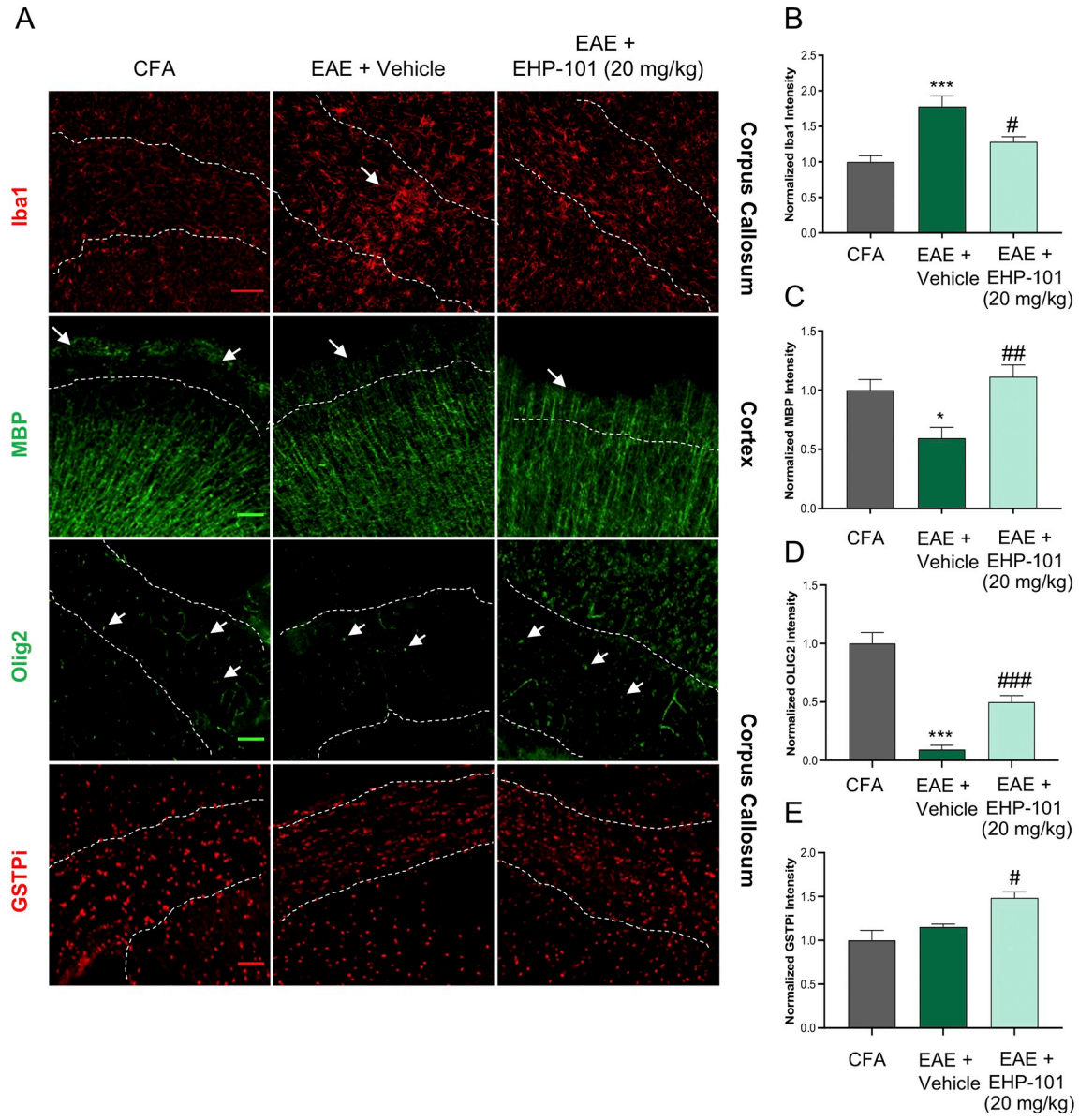

Fig. 3. Demyelination with persistent activation of microglia and loss of Olig2 expression was prevented by EHP-101 treatment. (**A**) Representative confocal microscopy images of immunolabeled cells for Iba1 (marked with arrow), MBP (arrowhead in panel), Olig2 (pointed by arrows) and GSTpi expression in corpus callosum and cortex. Scale bars equivalent to 100 μm. (**B-E**) The quantifications of each marker are shown as mean ± SEM (n = 5 animals per group), and significance was determined by one-way ANOVA followed by the Tukey's post-hoc test. *p < .05, ***p < .001 EAE + Vehicle vs CFA; #p < .05, ##p < .01, ###p < .001 EAE + EHP-101 vs EAE + Vehicle.

Chemokine Ligand 4 (Ccl4) and C–C Motif Chemokine Ligand 2 (Ccl2). We show in Fig. 4D that EHP-101 treatment downregulated the expression of these genes upregulated in EAE mice (Il6: p = .0360 EAE + Vehicle vs CFA; p = .0451 EAE + EHP-101 20 mg/kg vs EAE + Vehicle; Timp1: p = < 0.0001 EAE + Vehicle vs CFA; p = .0001 EAE + EHP-101 20 mg/kg vs EAE + Vehicle; VCAM: p = .0058 EAE + Vehicle vs CFA, p = .0381 EAE + EHP-101 20 mg/kg vs EAE + Vehicle; IL1b: p = .0018 EAE + Vehicle vs CFA; p = .0027 EAE + EHP-101 20 mg/kg vs EAE + Vehicle; Ccl4: p = < 0.0001 EAE + Vehicle vs CFA; p = < 0.0001 EAE + EHP-101 20 mg/kg vs EAE + Vehicle; Ccl2: p = .0003 EAE + Vehicle vs CFA; p = .0054 EAE + EHP-101 vs EAE + Vehicle), thus validating the results found in the RNA-Seq analysis.

Next, we performed a second analysis to explore changes in the opposite direction to the pattern shown by the pro-inflammatory genes. Thus, we selected down-regulated genes in the EAE vs control comparison and up-regulated in EAE + EHP-101 vs EAE comparison. We intersected both groups of genes to evaluate the overlap between them, resulting in a total of 193 genes downregulated in the untreated model that increased their expression in response to the treatment (Fig. 5A). Then we performed a second functional analysis, using the list of overlapping genes as input, to explore the most significantly enriched Gene Ontology (GO) terms. As depicted in Fig. 5B, we found several terms related to the metabolic process of sterols and hydroxy compounds at the top of the list. However, given the background of the disease, we decided to focus on the "myelination" process. To explore the changes of features belonging to this annotation, we depicted the expression levels of genes that produced this result in the heatmap shown in Fig. 5C. This allowed us to identify several key genes of the myelination process that were restoring their levels with EHP-101 treatment. Interestingly, these results indicated that EHP-101 normalized the expression of several genes associated with oligodendrocyte function, such as Gap junction gamma-3 (Gjc3), also called Connexin 29, and Teneurin-4 (Tenm4) that were downregulated in EAE. These

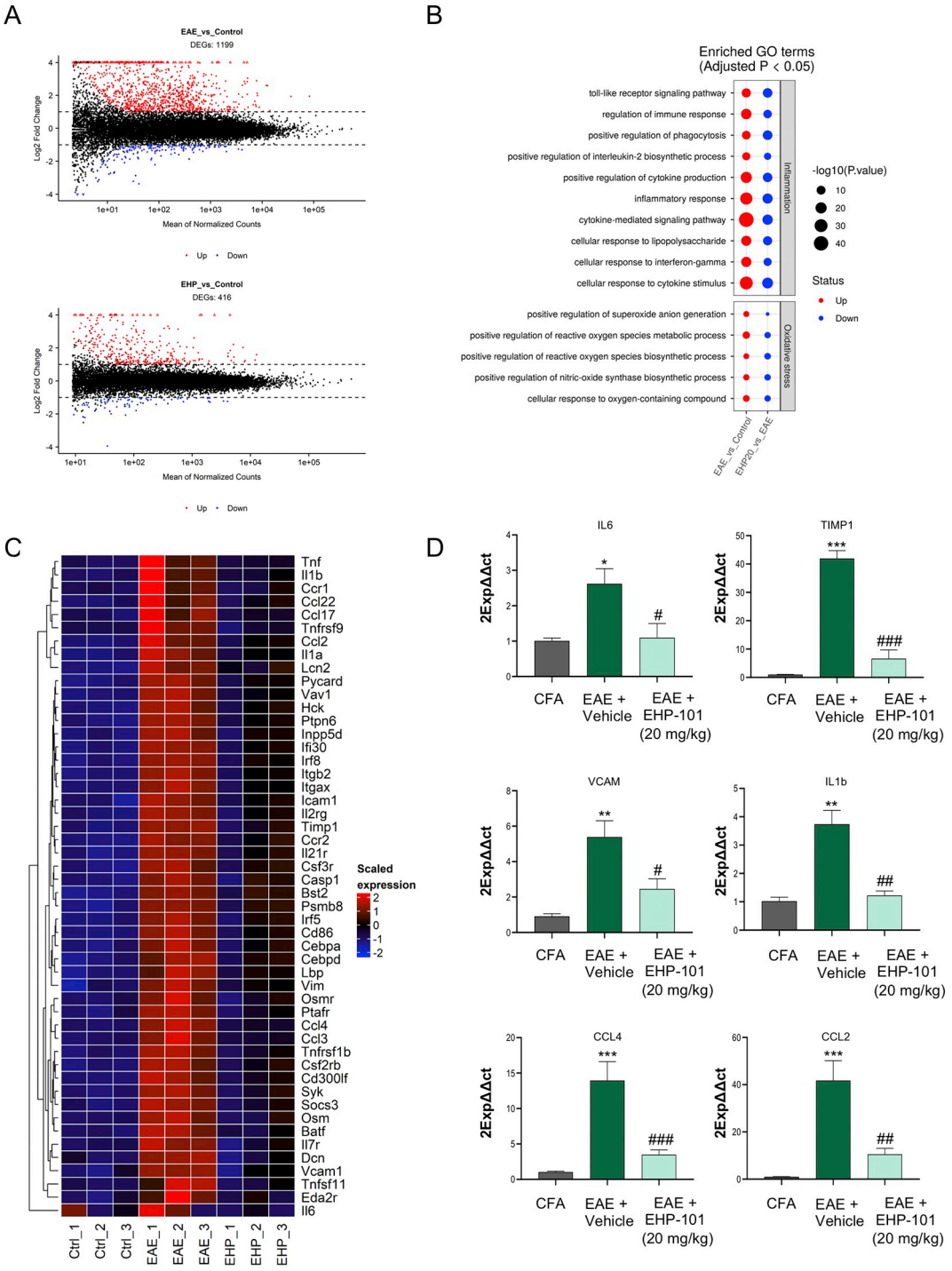

Fig. 4. Gene expression profiling of the effect of EHP-101 in EAE model. (**A**) MA plots of the EAE or EAE + EHP-101 vs control comparisons. The X axis represents the average expression as the mean of normalized counts while the Y axis indicates the magnitude of the change as the log2 transformed fold change. The color indicates genes that surpassed the cutoff of adjusted $P < .05$ and fold change < -2 (blue) or > 2 (red). **(B)** Over-representation analysis results for Gene Ontology (GO) terms related with inflammation and response to oxidative stress on genes up-regulated by EAE and down-regulated by the treatment. Dots indicate a significant over-representation (adjusted $P < .05$) of a Gene Ontology term (Y axis) for a given comparison (X-axis). **(C)** Heatmap depicting the expression levels for selected genes included in the "cytokine-mediated signaling pathway". **(D)** The mRNA expression for inflammatory marker in spinal cord (IL-6, Timp1, VCAM, IL1b, CCL2 and CCL4) was quantified by qPCR and normalized versus GAPDH. Data represent the mean ± SEM, and significance was determined by one-way ANOVA followed by the Tukey's post-hoc test. *p < .05, **p < .01, ***p < .001 EAE + Vehicle vs CFA; #p < .05, ##p < .01, ###p < .001 EAE + EHP-101 vs EAE + Vehicle. (For interpretation of the references to color in this figure legend, the reader is referred to the web version of this article.)

results are relevant since Tenm4 has been described as a critical regulator of oligodendrocyte differentiation and CNS myelination (Suzuki et al., 2012). To validate the transcriptomic analysis, we studied the expression of Gjc3 and Tenm4 by RT-PCR (Fig. 5D Tenm4: $p = .0020$ EAE + Vehicle vs CFA; $p = .0032$ EAE + EHP-101 20 mg/kg vs EAE + Vehicle; Gjc3: $p = .0006$ EAE + Vehicle vs CFA; $p = .0462$ EAE + EHP-101 20 mg/kg vs EAE + Vehicle) and the protein levels by IHC. As depicted in Fig. 5E (p = < 0.0001 EAE + Vehicle vs CFA:

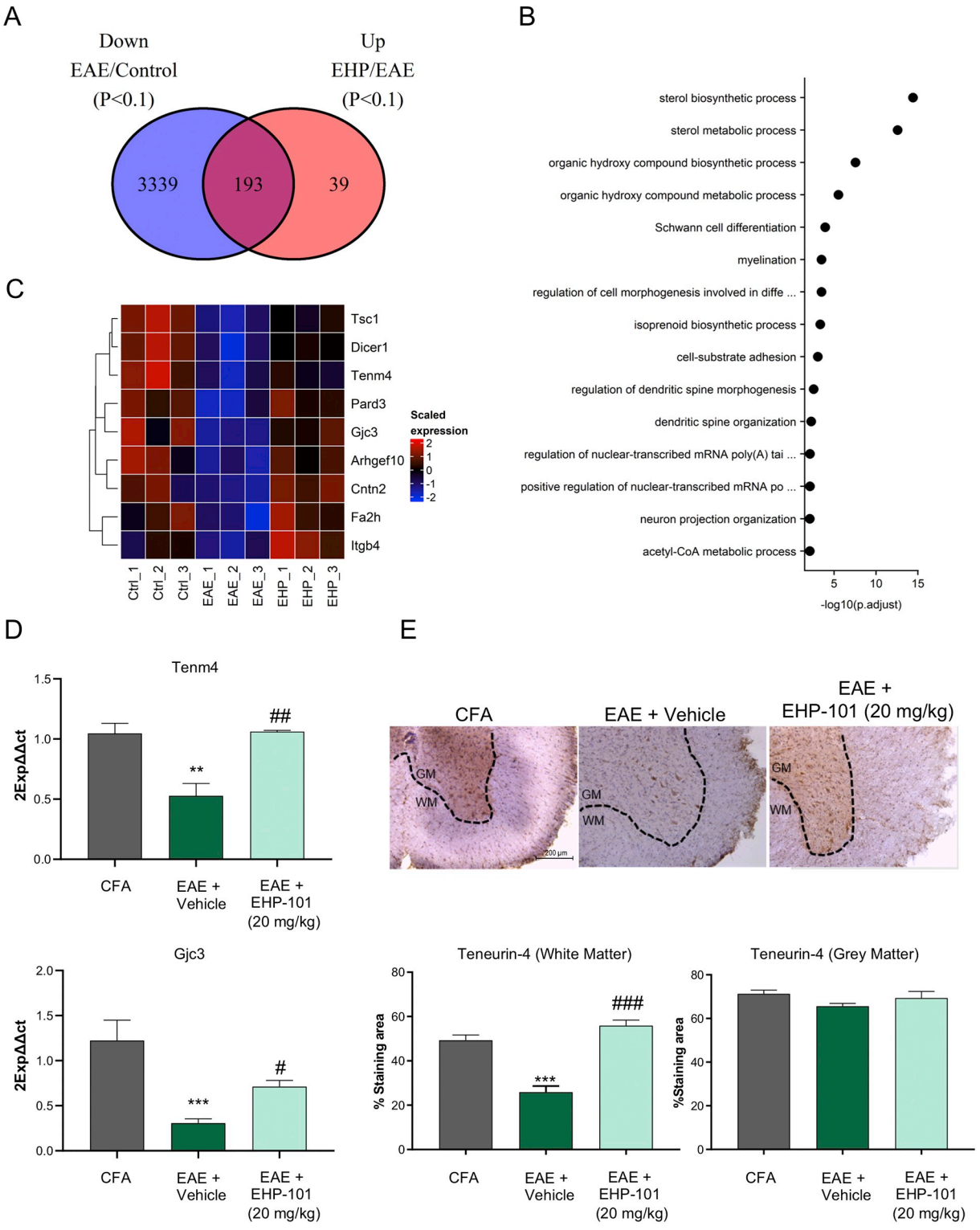

Fig. 5. EHP-101 treatment normalized the expression of genes associated with oligodendrocyte function. **(A)** Venn Diagram indicating the overlap between the sets of down regulated genes at EAE vs Control comparison (Adjusted $P < .1$ and fold change < 0) and up regulated genes at EAE + EHP-101 vs EAE comparison (Adjusted $P < .1$ and fold change > 0). **(B)** Functional analysis results for the set of 193 overlapping genes. The scatter plot represents the significance of the enrichment for the top 15 over-represented Gene Ontology (Biological Process) terms as the -log10 transformed adjusted *P* value. **(C)** Heatmap depicting the expression levels for genes annotated with the "myelination" GO term included in the set of 193 overlapping features. **(D)** The mRNA expression for myelination-related genes (Tenm4 and Gjc3) was quantified by qPCR and normalized versus GAPDH. **(E)** Immunohistochemistry labelling of spinal cord for Teneurin-4 in CFA, EAE+ + Vehicle and EAE + EHP-101 are shown. Scale bars equivalent to 200 µm. The quantification of expression of Teneurin-4 in the white and the gray matter (bottom panel). Data represent the mean ± SEM ($n = 5$ animals per group) and significance were determined by one-way ANOVA followed by the Tukey's post-hoc test. **p < .01, ***p < .001 EAE + Vehicle vs CFA; #p < .05, ##p < .01, ###p < .001 EAE + EHP-101 vs EAE + Vehicle.

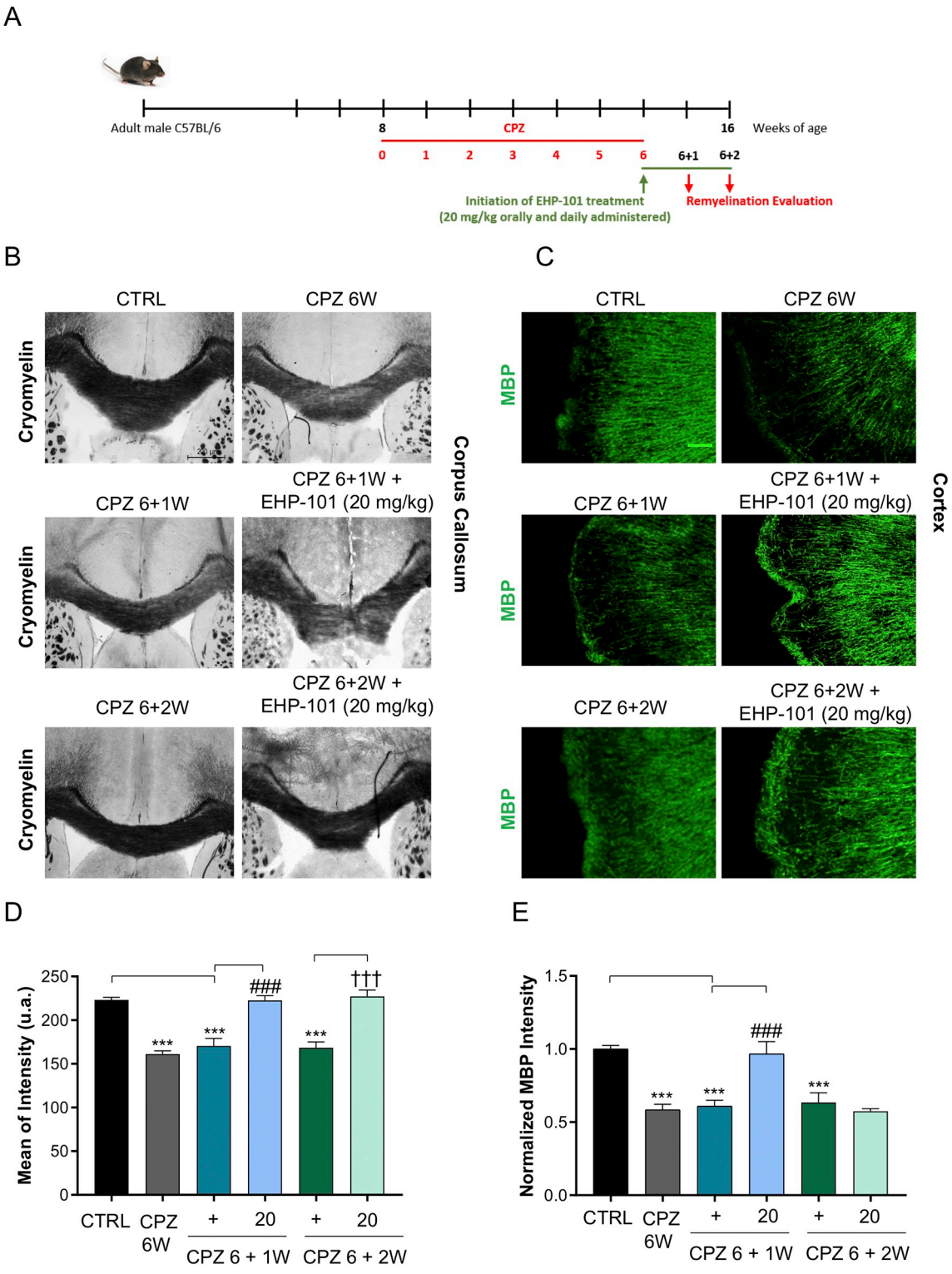

Fig. 6. Effect of EHP-101 treatment on remyelination in acute CPZ-induced demyelination. (**A**) Experimental procedure (**B**). Histological study of myelin by Cryomyelin staining in corpus callosum and quantification of the mean intensity is shown (**D**). (**C**) Immunodetection of MBP in the cerebral cortex, and (**E**) the quantification of MBP immunoreactivity. Scale bars equivalent to 200 μm (B) 100 μm (C). Data represent the mean ± SEM (n = 5 animals per group), and significance was determined by one-way ANOVA followed by the Tukey's post-hoc test. ***p < .001 CPZ 6 W or CPZ 6 W + 1 or CPZ 6 W + 2 vs Control; ###p < .001 CPZ 6 W +1 + EHP-101 vs CPZ 6 W +1, †††p < .001 CPZ 6 W +2 + EHP-101 vs CPZ 6 W +2.

p = < 0.0001 EAE + EHP-101 20 mg/kg vs EAE + Vehicle), a decrease of Tenm4 expression was observed in white matter of spinal cord compared to the CFA group which was prevented by EHP-101 treatment. Taken together, these results are indicative of the potential of EHP-101 to prevent demyelination in EAE model.

3.3. EHP-101 accelerates remyelination in cuprizone-challenged mice

To evaluate the effect of EHP-101 on remyelination during the acute CPZ-induced demyelination protocol (Fig. 6A), brain coronal sections from animals after 6 weeks of CPZ 0.2% diet and 2 weeks of EHP-101

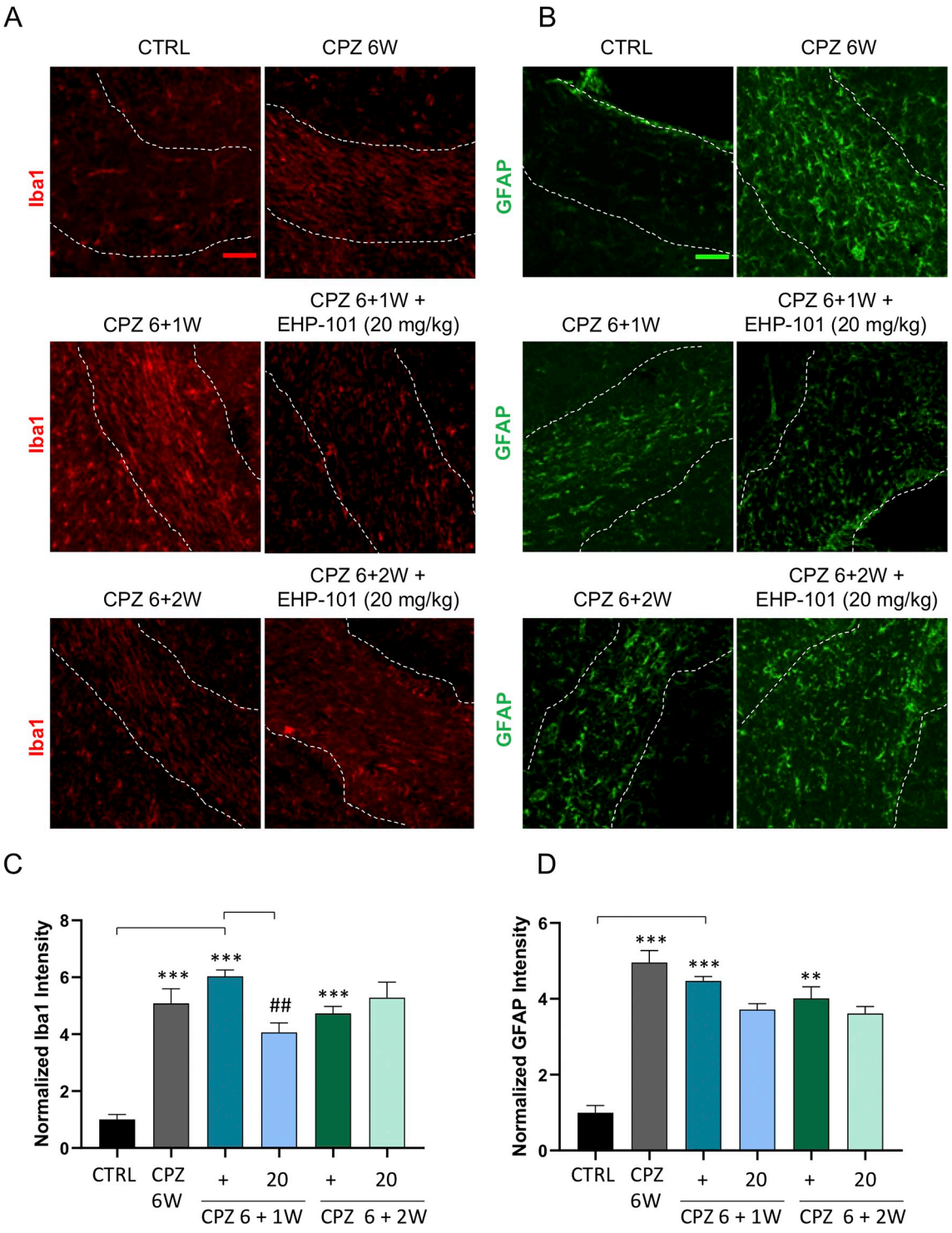

Fig. 7. Impact of EHP-101 treatment on microglia and astrocytes activation in acute CPZ-induced demyelination. (**A**) Expression of Iba1 in corpus callosum and quantification (**C**). (**B**) Astrogliosis was determined by immunofluorescence studies of GFAP in corpus callosum and quantification of intensity is shown (**D**). Scale bars equivalent to 100 μm. Data represent the mean ± SEM (n = 5 animals per group), and significance was determined by one-way ANOVA followed by the Tukey's post-hoc test. ***p < .001 CPZ 6 W or CPZ 6 W + 1 or CPZ 6 W + 2 vs Control; **p<0.01 CPZ 6 W + 2 vs Control; ##p < .01 CPZ 6 W +1 + EHP-101 vs CPZ 6 W +1.

treatment were evaluated. In this model, EHP-101 treatment was started after removal of the CPZ diet to study the effect of EHP-101 on spontaneous remyelination. First, the evaluation of MBP was determined by CryoMyelin and IHC staining (Fig. 6B and C, respectively). Spontaneous recovery from demyelination was insignificant after 1 and 2 weeks in untreated mice but remyelination was significantly accelerated by EHP-101 treatment in both the corpus callosum (Fig. 6D p = < 0.0001 CPZ6W, CPZ6 + 1 W, CPZ6 + 2 W vs Control; p = < 0.0001 CPZ6 + 1 W + EHP-101 20 mg/kg vs CPZ6 + 1 W; p = < 0.0001 CPZ6 + 2 W + EHP-101 20 mg/kg vs CPZ6 + 2 W) and the cerebral cortex (Fig. 6E p = < 0.0001 CPZ6W, CPZ6 + 1 W, CPZ6 + 2 W vs Control; p = < 0.0001 CPZ6 + 1 W + EHP-101

20 mg/kg vs CPZ6 + 1 W). Moreover, we investigated the effect of EHP-101 on neuroinflammation-associated glial activation by staining Iba-1$^+$ and GFAP$^+$ cells in the corpus callosum. In control mice, low expression levels of Iba-1$^+$ and GFAP$^+$ cells were detected but mice exposed to CPZ showed microglial and astrocytic activation, which was attenuated by EHP-101 treatment (Fig. 7A and B). Quantitative assessment also showed a significant increase in the number of Iba1$^+$ and GFAP$^+$ cells in corpus callosum upon CPZ intoxication. Microgliosis was ameliorated after 1 week of EHP-101 treatment and astrocytes activation also showed a tendency for inhibition (Fig. 7C $p = < 0.0001$ CPZ6W, CPZ6 + 1 W, CPZ6 + 2 W vs Control; $p = .0017$ CPZ6 + 1 W + EHP-101 20 mg/kg vs CPZ6 + 1 W; Fig. 7D $p = < 0.0001$ CPZ6W, CPZ6 + 1 W vs Control; $p = .0017$ CPZ6 + 2 W vs Control). To examine the effects of EHP-101 on cuprizone-induced demyelination of axons in the corpus callosum, we investigated the non-phosphorylated form of neurofilament proteins (SMI-32 staining). Although SMI-32 immunoreactivity is normally seen in axons, its accumulation in axonal spheroids is a characteristic of axonal pathology. Increased SMI-32 labeling after 6 and 7 weeks of CPZ intoxication demonstrated that there was a significant effect on axons and this effect was ameliorated after 1 week of EHP-101 treatment (Fig. 8).

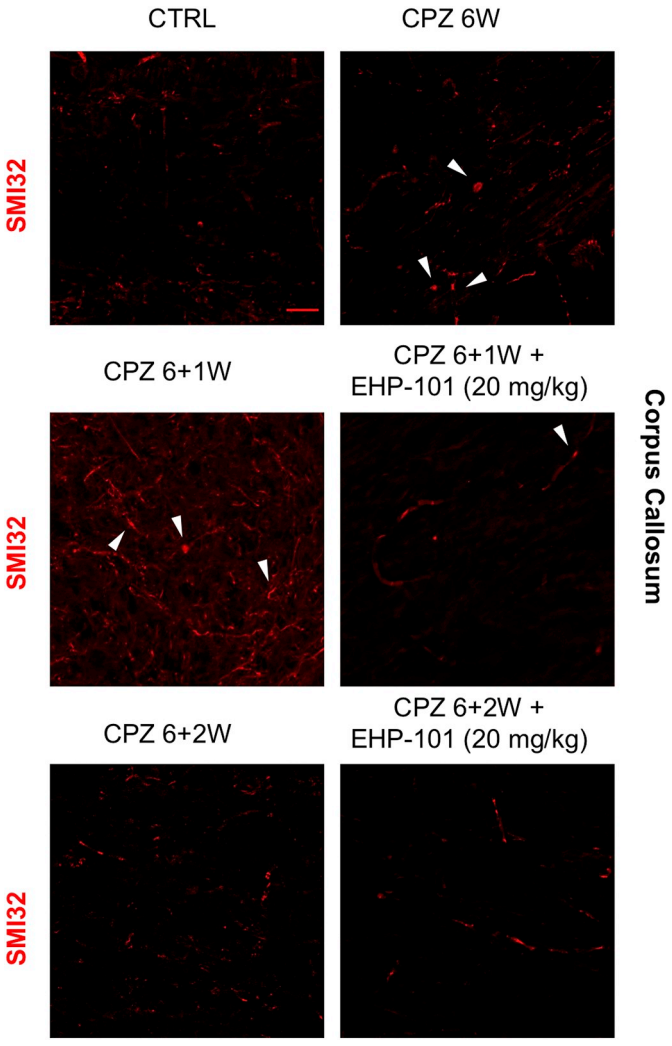

Fig. 8. EHP-101 reduces axonal degeneration induced by CPZ. Representative images of immunostaining of SMI-32$^+$ cells in the corpus callosum of different groups of animals (n = 5 animals per group). Axonal spheroids which are characteristic of axonal pathology are identified with white arrows. Scale bar equivalent to 20 μm.

4. Discussion

Natural products, including phytocannabinoids, have been successfully used for the development of synthetic and semisynthetic derivatives with improved bioactivities (Appendino et al., 2010). We have developed the compound VCE-004.8, a synthetic derivative of CBD, which is a dual agonist for PPARγ/CB_2 that also inhibits the activity of HIF prolyl hydroxylases (PHDs) (del Rio et al., 2016; Navarrete et al., 2018). Therefore, VCE-004.8 is targeting several pathways that may have a positive effect on neuroinflammation and remyelination as observed in EAE and Theiler's Murine Encephalomyelitis Virus-induced demyelinating models (Navarrete et al., 2018). Herein we have studied the effect of EHP-101, an oral lipidic formulation of VCE-004.8, in two of the most commonly used models of demyelination, which are EAE and toxically induced demyelination via cuprizone (Lassmann and Bradl, 2017).

EAE in C57BL/6 mice has generally been thought to predominantly target the spinal cord, leading to sensory and motor impairments. Nevertheless, it is also recognized that EAE involves other CNS structures including the cerebellum and the hippocampus (Brown and Sawchenko, 2007; MacKenzie-Graham et al., 2012). Our data clearly indicate that EHP-101 is effective in alleviating neuroinflammation in the spinal cord, in the cerebral cortex and in the corpus callosum. In the EAE model we cannot distinguish whether the effect of EHP-101 occurs in the peripheral immune system, in the CNS or both. It has been demonstrated that the blood-brain-barrier (BBB) can be disrupted in EAE allowing for the migration of autoimmune cells and molecules to the brain (Bennett et al., 2010). However, it is likely that EHP-101 may exert anti-inflammatory effects by acting both in the peripheral immune system and in the CNS. The formulation of VCE-004.8 in the selected vehicle (Corn oil and Maisine CC) may indeed explain the potential action of VCE-004.8 in the lymphatic nodes. Maisine CC is a long chain lipid ($C_{18:2}$) used to increase oral bioavailability and promote lymphatic absorption (Caliph et al., 2000; Khoo et al., 2003). Autoimmune diseases, including MS, are initiated in lymphoid tissues; furthermore, we have also demonstrated that EHP-101 showed anti-inflammatory and antifibrotic activities in a murine model of systemic sclerosis, another autoimmune disease where the BBB is not affected (Garcia-Martin et al., 2018). In addition, we show that EHP-101 alleviates neuroinflammation in CPZ-intoxicated mice. This model is considered independent of T cells and B cells because RAG^{-}/$^{-}$ mice show no difference in demyelination or remyelination (Arnett et al., 2001). CPZ-induced demyelinating lesions are characterized by severe oligodendrocyte loss and demyelination with concomitant activation of microglia and astrocytes, but they do not induce BBB damage (Bakker and Ludwin, 1987; Kondo et al., 1987; McMahon et al., 2002) and lack the characteristic T-cell infiltration and consequently the peripheral autoimmune component of the disease (Kipp et al., 2009).

Extensive experimental studies have revealed that activating HIF-1α by inhibiting the activation of PHDs can provide neuroprotection and perhaps remyelination mainly from the increased expression of HIF-1 target genes, which combat oxidative stress, improve blood oxygen and glucose supply, promote glucose metabolism, regulate iron homeostasis and block cell death signal pathways. Increasing HIF-1 activity may be an important potential strategy to prevent the onset or to ameliorate the pathogenesis of neurodegenerative diseases (Zhang et al., 2011). In fact, activation of the HIF-1 pathway by hypoxia preconditioning process induced by mild oxygen depletion is beneficial in a wide number of neurological disorders, including MS (Esen et al., 2013; Stetler et al., 2014). Interestingly, a recent report has shown that mild hypoxia promotes recovery from preexisting inflammatory demyelinating disease and suggesting that this protection may be the result of enhanced vascular integrity and accelerated apoptosis of infiltrated monocytes (Halder and Milner, 2020). The cellular adaptation to severe or mild hypoxia is very fast and involves the activation of the hypoxia-inducible factor (HIF)-1α, whose activation may play a role in the inflammatory

and the remitting phases of MS (reviewed by (Girolamo et al., 2014)). Remarkably, the improvement of the myelination index was paralleled by enhancement of oligodendrocyte progenitor cell (OPC) proliferation, platelet-derived growth factor (PDGF)α-receptor expression, and precursor migration from the CC midline to the lateral parts followed by an induction of the expression of myelin protein (Patel and Klein, 2011). In addition, early astrogliosis in the demyelinated areas paralleled a moderate stimulation of insulin-like growth factor (IGF)-1 expression (Kipp et al., 2009). IGF-1 synergizes with fibroblast growth factor (FGF)-2 to stimulate oligodendrocyte progenitor entry into the cell cycle (Jiang et al., 2001). This is of particular interest because IGF-1 induced HIF-1 activation that could be mimicked by VCE-004.8 in the brain, and PDGFα and FGF2 are also regulated by VCE-004.8-mediated activation of the HIF pathway (Calvani et al., 2006; Navarrete et al., 2018; Schito et al., 2012). Nevertheless, the mechanism of action of EHP-101 in the remyelination process is still unknown. Although in our transcriptomic analysis in the spinal cord of EAE mice we could not find an upregulation of genes directly regulated by HIF-1α we cannot discard that it could be related to the activation of this pathway by acting on nearby tissues such as endothelial vascular cells. Further experiments are required to confirm the involvement of HIF-1α in the efficacy of EHP-101 on remyelination.

Demyelination and partial axonal damage in MS lesions are closely associated with reactive activation of microglial cells which are seen in close contact with axons, that reveal acute axonal injury, such as the formation of axonal spheroids or a disturbance of fast axonal transport (Ferguson et al., 1997; Trapp et al., 1998). Reactive microglia produce a large array of toxic and proinflammatory molecules, which triggers myelin destruction, oligodendrocyte deterioration, axon damage and even neuronal loss (Popescu and Lucchinetti, 2012) (Song and Suk, 2017). Here we found that oral EHP-101 also prevented microglia activation and demyelination in both spinal cord and brain, suggesting that part of this effect could be mediated by the penetration of VCE-004.8 in the brains of EAE mice. Moreover, we also found that EHP-101 preserves the axonal structure ameliorating the typical accumulation of spheroids of SMI-32 used as a marker of axonal damage in CPZ intoxicated mice (Peterson et al., 2001; Trapp et al., 1998; Werner et al., 2001). Again, this result suggests that VCE-004.8 can also cross the BBB, which is not affected in the CPZ model (Bakker and Ludwin, 1987). However, we do not have direct measurement of the compound in the brain of EAE and CPZ mice and further experiment are required to validate this possibility.

Oligodendrocyte progenitor cells (OPCs) are produced from neuroepithelial stem cells and subsequently proliferate and migrate throughout the entire spinal cord (Tsai et al., 2009). During differentiation, oligodendrocytes initiate expression of myelin proteins critical for the achievement of proper functioning of the CNS (Louis et al., 1992). Teneurin-4 (Tenm4) is a type II transmembrane protein that is highly expressed in the CNS and whose expression is induced in response to endoplasmic reticulum stress (Wang et al., 1998) and has been suggested to be involved in bipolar disorder in humans (Psychiatric, 2011). A mouse mutation, designated *furue*, which results in tremors and severe hypomyelination of small-diameter axons, reduces oligodendrocyte differentiation especially in the spinal cord of the CNS, and it has been associated with the absence of Tenm4 expression. Thus, Tenm4 is a critical regulator of oligodendrocyte differentiation and CNS myelination (Suzuki et al., 2012). Herein we showed for the first time that in EAE mice the expression of Tenm4 is downregulated in the spinal cord and the treatment with EHP-101 reverses this downregulation probably as a result of the anti-inflammatory activity of VCE-004.8.

In addition, oligodendrocytes are electrically and metabolically coupled through intercellular channels called gap junctions (GJs), composed of connexins Cx29, Cx32 and Cx47 (Kleopa et al., 2004), with other oligodendrocytes as well as with astrocytes. This glial network of communication plays an important role in the homeostasis of brain function (Giaume et al., 2010; Orthmann-Murphy et al., 2008). Several studies have also provided the role of oligodendrocyte connexins in acquired demyelinating CNS disorders, in particular MS and related experimental models (Markoullis et al., 2012a; Markoullis et al., 2012b). They also appear to have a regulatory role in neuroinflammation as their absence further aggravates inflammatory demyelination (Papaneophytou et al., 2018). Again, our results demonstrated that EHP-101 prevented the downregulation of Gjc3 (connexin 29) expression in EAE mice vs control mice. In light of the relevance of Tenm4 and Gjc3 for oligodendrocyte function and myelin preservation, our results further support the potential of EHP-101 to be developed as a novel treatment of MS.

5. Conclusions

In conclusion, we have shown the protective effect of EHP-101 against demyelination and its capability to enhance remyelination. These results open new strategies for the treatment of MS and other demyelinating diseases, since novel therapies aimed at axonal remyelination are urgently needed.

Ethics approval and consent to participate

All experiments with laboratory animals were conducted according to European guidelines (directive 2010/63/EU), and the Ethics Committees on Animal Experimentation at the Cajal Institute (CSIC, Madrid) and the University of Córdoba (Córdoba, Spain) approved all the procedures described in this study (protocol numbers: 962013/03 CEEA-IC and 2018PI/02 (UCO).

Consent for publication

Not applicable.

Availability of data and material

Gene Expression Omnibus databank (accession no. GSE131854).

Credit author statement

Carmen Navarrete, Adela García-Martín, Leyre Mestre and Ana Feliú performed in vivo experiments. Carmen Guaza and Eduardo Muñoz managed and designed the overall study. Martín Garrido-Rodriguez and Marco A. Calzado performed the bioinformatic analysis. Carmen Navarrete, Adela García-Martín and Martín Garrido-Rodriguez performed statistical analysis. Carmen Navarrete and Eduardo Muñoz wrote the manuscript. All the authors approved the final manuscript.

Funding

This work was supported by grants SAF2017–87701-R (EM), SAF2016–76449-R (GC) from the Ministry of the Economy and Competition (MINECO) co-financed with the European Union FEDER funds. GC was also supported by the Red Española de Esclerosis Múltiple (REEM: RD16/0015/0021) sponsored by the Fondo de Investigación Sanitaria (FIS) (GC). This work was also partially supported by Emerald Health Pharmaceuticals (San Diego, USA).

Author contributions

CN, AGM, LM, and AF performed in vivo experiments. GC and EM managed and designed the overall study. MGR and MAC performed the bioinformatic analysis. CN, AGM and MGR performed statistical analysis. CN and EM wrote the manuscript. All the authors approved the final manuscript.

Declaration of Competing Interest

Carmen Navarrete is an employee of Emerald Health Pharmaceuticals. Adela García-Martin is an employee of Emerald Health Biotechnology. Eduardo Muñoz is Chief Scientific Officer of Emerald Health Pharmaceuticals and a member of the Scientific Advisory Boards of Emerald Health Pharmaceuticals and Emerald Health Biotechnology.

Acknowledgements

We thank Carmen-Cabrero for revising the manuscript.

Appendix A

Table A.1
Primers used in real-time PCR analysis.

Genes	Forward (5′—3′)	Reverse (5′—3′)
IL-6	GTATGAACAACGATGATGCACTTG	ATGGTACTCCAGAAGACCAGAGGA
IL-1b	CTCCACCTCAATGGACAGAA	GCCGTCTTTCATTACACAGG
CCL2	GGGCCTGCTGTTCACAGTT	CCAGCCTACTCATTGGGAT
CCL4	AGAAACAGCAGGAAGTGGGA	AACACCATGAAGCTCTGCGT
Gjc3	ATGTGCGGCAGGTTCCTGAGACA	TCAAAATGGCTCTTTTGCCTCCA
TIMP1	TCCTCTTGTTGCTATCACTGATAGCTT	CGCTGGTATAAGGTGGTCTCGTT
Tenm4	GTGGACAAGTTTGGGCTCATTTAT	GGGTTGATGGCTAAGTCTGTGG
VCAM	AGTTGGGGATTCGGTTGTTC	CATTCCTTACCACCCCATTG
GAPDH	TGGCAAAGTGGAGATTGTTGCC	AAGATGGTGATGGGCTTCCCG

References

Appendino, G., et al., 2010. Comprehensive Natural Products II Chemistry and Biology Natural Products Drug Discovery. 3. pp. 205–236.
Arnett, H.A., et al., 2001. TNF alpha promotes proliferation of oligodendrocyte progenitors and remyelination. Nat. Neurosci. 4, 1116–1122. https://doi.org/10.1038/nn738.
Bakker, D.A., Ludwin, S.K., 1987. Blood-brain barrier permeability during Cuprizone-induced demyelination. Implications for the pathogenesis of immune-mediated demyelinating diseases. J. Neurol. Sci. 78, 125–137. https://doi.org/10.1016/0022-510x(87)90055-4.
Barrie, N., Manolios, N., 2017. The endocannabinoid system in pain and inflammation: its relevance to rheumatic disease. Eur J Rheumatol. 4, 210–218. https://doi.org/10.5152/eurjrheum.2017.17025.
Bennett, J., et al., 2010. Blood-brain barrier disruption and enhanced vascular permeability in the multiple sclerosis model EAE. J. Neuroimmunol. 229, 180–191. https://doi.org/10.1016/j.jneuroim.2010.08.011.
Bernal-Chico, A., et al., 2015. Blockade of monoacylglycerol lipase inhibits oligodendrocyte excitotoxicity and prevents demyelination in vivo. Glia. 63, 163–176. https://doi.org/10.1002/glia.22742.
Bernardo, A., Minghetti, L., 2006. PPAR-gamma agonists as regulators of microglial activation and brain inflammation. Curr. Pharm. Des. 12, 93–109. https://doi.org/10.2174/138161206780574579.
Bernardo, A., et al., 2009. Peroxisome proliferator-activated receptor-gamma agonists promote differentiation and antioxidant defenses of oligodendrocyte progenitor cells. J. Neuropathol. Exp. Neurol. 68, 797–808. https://doi.org/10.1097/NEN.0b013e3181aba2c1.
Bolger, A.M., et al., 2014. Trimmomatic: a flexible trimmer for Illumina sequence data. Bioinformatics. 30, 2114–2120. https://doi.org/10.1093/bioinformatics/btu170.
Bonzano, L., et al., 2008. Callosal contributions to simultaneous bimanual finger movements. J. Neurosci. 28, 3227–3233. https://doi.org/10.1523/JNEUROSCI.4076-07.2008.
Brodbeck, J., et al., 2008. Rosiglitazone increases dendritic spine density and rescues spine loss caused by apolipoprotein E4 in primary cortical neurons. Proc. Natl. Acad. Sci. U. S. A. 105, 1343–1346. https://doi.org/10.1073/pnas.0709906104.
Brown, D.A., Sawchenko, P.E., 2007. Time course and distribution of inflammatory and neurodegenerative events suggest structural bases for the pathogenesis of experimental autoimmune encephalomyelitis. J. Comp. Neurol. 502, 236–260. https://doi.org/10.1002/cne.21307.
Caliph, S.M., et al., 2000. Effect of short-, medium-, and long-chain fatty acid-based vehicles on the absolute oral bioavailability and intestinal lymphatic transport of halofantrine and assessment of mass balance in lymph-cannulated and non-cannulated rats. J. Pharm. Sci. 89, 1073–1084. https://doi.org/10.1002/1520-6017(200008)89:8<1073::aid-jps12>3.0.co;2-v.
Calvani, M., et al., 2006. Hypoxic induction of an HIF-1alpha-dependent bFGF autocrine loop drives angiogenesis in human endothelial cells. Blood. 107, 2705–2712. https://doi.org/10.1182/blood-2005-09-3541.
Chiurchiu, V., et al., 2018. The endocannabinoid system and its therapeutic exploitation in multiple sclerosis: clues for other neuroinflammatory diseases. Prog. Neurobiol. 160, 82–100. https://doi.org/10.1016/j.pneurobio.2017.10.007.
Daynes, R.A., Jones, D.C., 2002. Emerging roles of PPARs in inflammation and immunity. Nat. Rev. Immunol. 2, 748–759. https://doi.org/10.1038/nri912.
De Nuccio, C., et al., 2011. Peroxisome proliferator-activated receptor gamma agonists accelerate oligodendrocyte maturation and influence mitochondrial functions and oscillatory ca(2+) waves. J. Neuropathol. Exp. Neurol. 70, 900–912. https://doi.org/10.1097/NEN.0b013e3182309ab1.
del Rio, C., et al., 2016. The cannabinoid quinol VCE-004.8 alleviates bleomycin-induced scleroderma and exerts potent antifibrotic effects through peroxisome proliferator-activated receptor-gamma and CB2 pathways. Sci. Rep. 6, 21703. https://doi.org/10.1038/srep21703.
Esen, N., et al., 2013. Induction of vascular remodeling: a novel therapeutic approach in EAE. J. Neurol. Sci. 333, 88–92. https://doi.org/10.1016/j.jns.2013.06.004.
Feliu, A., et al., 2017. 2-Arachidonoylglycerol reduces proteoglycans and enhances remyelination in a progressive model of demyelination. J. Neurosci. 37, 8385–8398. https://doi.org/10.1523/JNEUROSCI.2900-16.2017.
Ferguson, B., et al., 1997. Axonal damage in acute multiple sclerosis lesions. Brain. 120 (Pt 3), 393–399. https://doi.org/10.1093/brain/120.3.393.
Fox, R.J., et al., 2015. Comparative effectiveness using a matching-adjusted indirect comparison between delayed-release dimethyl fumarate and Fingolimod for the treatment of relapsing-remitting multiple sclerosis. Value Health 18, A750. https://doi.org/10.1016/j.jval.2015.09.2902.
Garcia-Martin, A., et al., 2018. EHP-101, an oral formulation of the cannabidiol aminoquinone VCE-004.8, alleviates bleomycin-induced skin and lung fibrosis. Biochem. Pharmacol. 157, 304–313. https://doi.org/10.1016/j.bcp.2018.07.047.
Garcia-Martin, A., et al., 2019. Cannabinoid derivatives acting as dual PPARgamma/CB2 agonists as therapeutic agents for systemic sclerosis. Biochem. Pharmacol. 163, 321–334. https://doi.org/10.1016/j.bcp.2019.02.029.
Giaume, C., et al., 2010. Astroglial networks: a step further in neuroglial and gliovascular interactions. Nat. Rev. Neurosci. 11, 87–99. https://doi.org/10.1038/nrn2757.
Girolamo, F., et al., 2014. Angiogenesis in multiple sclerosis and experimental autoimmune encephalomyelitis. Acta Neuropathol Commun. 2, 84. https://doi.org/10.1186/s40478-014-0084-z.
Halder, S.K., Milner, R., 2020. Chronic mild hypoxia accelerates recovery from pre-existing EAE by enhancing vascular integrity and apoptosis of infiltrated monocytes. Proc. Natl. Acad. Sci. U. S. A. 117, 11126–11135. https://doi.org/10.1073/pnas.1920935117.
Ilyasov, A.A., et al., 2018. The endocannabinoid system and oligodendrocytes in health and disease. Front. Neurosci. 12, 733. https://doi.org/10.3389/fnins.2018.00733.
Inestrosa, N.C., et al., 2005. Peroxisome proliferator-activated receptor gamma is expressed in hippocampal neurons and its activation prevents beta-amyloid neurodegeneration: role of Wnt signaling. Exp. Cell Res. 304, 91–104. https://doi.org/10.1016/j.yexcr.2004.09.032.
Jiang, F., et al., 2001. IGF-I synergizes with FGF-2 to stimulate oligodendrocyte progenitor entry into the cell cycle. Dev. Biol. 232, 414–423. https://doi.org/10.1006/dbio.2001.0208.
Kanakasabai, S., et al., 2012. PPARgamma agonists promote oligodendrocyte differentiation of neural stem cells by modulating stemness and differentiation genes. PLoS One 7, e50500. https://doi.org/10.1371/journal.pone.0050500.
Khoo, S.M., et al., 2003. Intestinal lymphatic transport of halofantrine occurs after oral administration of a unit-dose lipid-based formulation to fasted dogs. Pharm. Res. 20, 1460–1465. https://doi.org/10.1023/a:1025718513246.
Kim, D., et al., 2015. HISAT: a fast spliced aligner with low memory requirements. Nat. Methods 12, 357–360. https://doi.org/10.1038/nmeth.3317.
Kipp, M., et al., 2009. The cuprizone animal model: new insights into an old story. Acta Neuropathol. 118, 723–736. https://doi.org/10.1007/s00401-009-0591-3.
Kister, I., et al., 2013. Disability in multiple sclerosis: a reference for patients and clinicians. Neurology. 80, 1018–1024. https://doi.org/10.1212/WNL.0b013e3182872855.
Kleopa, K.A., et al., 2004. Unique distributions of the gap junction proteins connexin29,

connexin32, and connexin47 in oligodendrocytes. Glia. 47, 346–357. https://doi.org/10.1002/glia.20043.
Klipper-Aurbach, Y., et al., 1995. Mathematical formulae for the prediction of the residual beta cell function during the first two years of disease in children and adolescents with insulin-dependent diabetes mellitus. Med. Hypotheses 45, 486–490.
Kondo, A., et al., 1987. Blood-brain barrier permeability to horseradish peroxidase in twitcher and cuprizone-intoxicated mice. Brain Res. 425, 186–190. https://doi.org/10.1016/0006-8993(87)90499-9.
Kong, W., et al., 2014. Selective CB2 receptor activation ameliorates EAE by reducing Th17 differentiation and immune cell accumulation in the CNS. Cell. Immunol. 287, 1–17. https://doi.org/10.1016/j.cellimm.2013.11.002.
Kornek, B., Lassmann, H., 2003. Neuropathology of multiple sclerosis-new concepts. Brain Res. Bull. 61, 321–326.
Kuleshov, M.V., et al., 2016. Enrichr: a comprehensive gene set enrichment analysis web server 2016 update. Nucleic Acids Res. 44, W90–W97. https://doi.org/10.1093/nar/gkw377.
Lassmann, H., 2010. Axonal and neuronal pathology in multiple sclerosis: what have we learnt from animal models. Exp. Neurol. 225, 2–8. https://doi.org/10.1016/j.expneurol.2009.10.009.
Lassmann, H., Bradl, M., 2017. Multiple sclerosis: experimental models and reality. Acta Neuropathol. 133, 223–244. https://doi.org/10.1007/s00401-016-1631-4.
Liao, Y., et al., 2014. featureCounts: an efficient general purpose program for assigning sequence reads to genomic features. Bioinformatics. 30, 923–930. https://doi.org/10.1093/bioinformatics/btt656.
Louis, J.C., et al., 1992. CG-4, a new bipotential glial cell line from rat brain, is capable of differentiating in vitro into either mature oligodendrocytes or type-2 astrocytes. J. Neurosci. Res. 31, 193–204. https://doi.org/10.1002/jnr.490310125.
Love, M.I., et al., 2014. Moderated estimation of fold change and dispersion for RNA-seq data with DESeq2. Genome Biol. 15, 550. https://doi.org/10.1186/s13059-014-0550-8.
Luna-Medina, R., et al., 2005. Regulation of inflammatory response in neural cells in vitro by thiadiazolidinones derivatives through peroxisome proliferator-activated receptor gamma activation. J. Biol. Chem. 280, 21453–21462. https://doi.org/10.1074/jbc.M414390200.
MacKenzie-Graham, A., et al., 2012. Cortical atrophy in experimental autoimmune encephalomyelitis: in vivo imaging. Neuroimage. 60, 95–104. https://doi.org/10.1016/j.neuroimage.2011.11.099.
Manson, S.C., et al., 2006. Loss of interhemispheric inhibition in patients with multiple sclerosis is related to corpus callosum atrophy. Exp. Brain Res. 174, 728–733. https://doi.org/10.1007/s00221-006-0517-4.
Manson, S.C., et al., 2008. Impairment of movement-associated brain deactivation in multiple sclerosis: further evidence for a functional pathology of interhemispheric neuronal inhibition. Exp. Brain Res. 187, 25–31. https://doi.org/10.1007/s00221-008-1276-1.
Markoullis, K., et al., 2012a. Disruption of oligodendrocyte gap junctions in experimental autoimmune encephalomyelitis. Glia. 60, 1053–1066. https://doi.org/10.1002/glia.22334.
Markoullis, K., et al., 2012b. Gap junction pathology in multiple sclerosis lesions and normal-appearing white matter. Acta Neuropathol. 123, 873–886. https://doi.org/10.1007/s00401-012-0978-4.
McFarland, H.F., Martin, R., 2007. Multiple sclerosis: a complicated picture of autoimmunity. Nat. Immunol. 8, 913–919. https://doi.org/10.1038/ni1507.
McMahon, E.J., et al., 2002. Peripheral macrophage recruitment in cuprizone-induced CNS demyelination despite an intact blood-brain barrier. J. Neuroimmunol. 130, 32–45. https://doi.org/10.1016/s0165-5728(02)00205-9.
Navarrete, C., et al., 2018. Hypoxia mimetic activity of VCE-004.8, a cannabidiol quinone derivative: implications for multiple sclerosis therapy. J. Neuroinflammation 15, 64. https://doi.org/10.1186/s12974-018-1103-y.
Orthmann-Murphy, J.L., et al., 2008. Gap junctions couple astrocytes and oligodendrocytes. J. Mol. Neurosci. 35, 101–116. https://doi.org/10.1007/s12031-007-9027-5.
Pacher, P., Kunos, G., 2013. Modulating the endocannabinoid system in human health and disease–successes and failures. FEBS J. 280, 1918–1943. https://doi.org/10.1111/febs.12260.
Pacher, P., Mechoulam, R., 2011. Is lipid signaling through cannabinoid 2 receptors part of a protective system? Prog. Lipid Res. 50, 193–211. https://doi.org/10.1016/j.plipres.2011.01.001.
Papaneophytou, C.P., et al., 2018. Regulatory role of oligodendrocyte gap junctions in inflammatory demyelination. Glia. 66, 2589–2603. https://doi.org/10.1002/glia.23513.
Patel, J.R., Klein, R.S., 2011. Mediators of oligodendrocyte differentiation during remyelination. FEBS Lett. 585, 3730–3737. https://doi.org/10.1016/j.febslet.2011.04.037.
Peterson, J.W., et al., 2001. Transected neurites, apoptotic neurons, and reduced inflammation in cortical multiple sclerosis lesions. Ann. Neurol. 50, 389–400. https://doi.org/10.1002/ana.1123.
Pistis, M., O'Sullivan, S.E., 2017. The role of nuclear hormone receptors in cannabinoid function. Adv. Pharmacol. 80, 291–328. https://doi.org/10.1016/bs.apha.2017.03.008.
Popescu, B.F., Lucchinetti, C.F., 2012. Pathology of demyelinating diseases. Annu. Rev. Pathol. 7, 185–217. https://doi.org/10.1146/annurev-pathol-011811-132443.
Psychiatric, G. C. B. D. W. G, 2011. Large-scale genome-wide association analysis of bipolar disorder identifies a new susceptibility locus near ODZ4. Nat. Genet. 43, 977–983. https://doi.org/10.1038/ng.943.
Rasmussen, S., et al., 2007. Persistent activation of microglia is associated with neuronal dysfunction of callosal projecting pathways and multiple sclerosis-like lesions in relapsing–remitting experimental autoimmune encephalomyelitis. Brain. 130, 2816–2829. https://doi.org/10.1093/brain/awm219.
Ricote, M., et al., 1998a. Expression of the peroxisome proliferator-activated receptor gamma (PPARgamma) in human atherosclerosis and regulation in macrophages by colony stimulating factors and oxidized low density lipoprotein. Proc. Natl. Acad. Sci. U. S. A. 95, 7614–7619. https://doi.org/10.1073/pnas.95.13.7614.
Ricote, M., et al., 1998b. The peroxisome proliferator-activated receptor-gamma is a negative regulator of macrophage activation. Nature. 391, 79–82. https://doi.org/10.1038/34178.
Roth, A.D., et al., 2003. PPAR gamma activators induce growth arrest and process extension in B12 oligodendrocyte-like cells and terminal differentiation of cultured oligodendrocytes. J. Neurosci. Res. 72, 425–435. https://doi.org/10.1002/jnr.10596.
Sanchez, A.J., Garcia-Merino, A., 2012. Neuroprotective agents: cannabinoids. Clin. Immunol. 142, 57–67. https://doi.org/10.1016/j.clim.2011.02.010.
Schito, L., et al., 2012. Hypoxia-inducible factor 1-dependent expression of platelet-derived growth factor B promotes lymphatic metastasis of hypoxic breast cancer cells. Proc. Natl. Acad. Sci. U. S. A. 109, E2707–E2716. https://doi.org/10.1073/pnas.1214019109.
Scolding, N., Franklin, R., 1998. Axon loss in multiple sclerosis. Lancet. 352, 340–341. https://doi.org/10.1016/S0140-6736(05)60463-1.
Song, G.J., Suk, K., 2017. Pharmacological modulation of functional phenotypes of microglia in neurodegenerative diseases. Front. Aging Neurosci. 9, 139. https://doi.org/10.3389/fnagi.2017.00139.
Stetler, R.A., et al., 2014. Preconditioning provides neuroprotection in models of CNS disease: paradigms and clinical significance. Prog. Neurobiol. 114, 58–83. https://doi.org/10.1016/j.pneurobio.2013.11.005.
Storch, M.K., et al., 2006. Cortical demyelination can be modeled in specific rat models of autoimmune encephalomyelitis and is major histocompatibility complex (MHC) haplotype-related. J. Neuropathol. Exp. Neurol. 65, 1137–1142. https://doi.org/10.1097/01.jnen.0000248547.13176.9d.
Storer, P.D., et al., 2005. Peroxisome proliferator-activated receptor-gamma agonists inhibit the activation of microglia and astrocytes: implications for multiple sclerosis. J. Neuroimmunol. 161, 113–122. https://doi.org/10.1016/j.jneuroim.2004.12.015.
Straus, D.S., Glass, C.K., 2007. Anti-inflammatory actions of PPAR ligands: new insights on cellular and molecular mechanisms. Trends Immunol. 28, 551–558. https://doi.org/10.1016/j.it.2007.09.003.
Suzuki, N., et al., 2012. Teneurin-4 is a novel regulator of oligodendrocyte differentiation and myelination of small-diameter axons in the CNS. J. Neurosci. 32, 11586–11599. https://doi.org/10.1523/JNEUROSCI.2045-11.2012.
Tomas-Roig, J., et al., 2016. The cannabinoid CB1/CB2 agonist WIN55212.2 promotes oligodendrocyte differentiation in vitro and neuroprotection during the Cuprizone-induced central nervous system demyelination. CNS Neurosci Ther. 22, 387–395. https://doi.org/10.1111/cns.12506.
Trapp, B.D., et al., 1998. Axonal transection in the lesions of multiple sclerosis. N. Engl. J. Med. 338, 278–285. https://doi.org/10.1056/NEJM199801293380502.
Tsai, H.H., et al., 2009. Distinct modes of migration position oligodendrocyte precursors for localized cell division in the developing spinal cord. J. Neurosci. Res. 87, 3320–3330. https://doi.org/10.1002/jnr.22058.
Wang, X.Z., et al., 1998. Identification of novel stress-induced genes downstream of chop. EMBO J. 17, 3619–3630. https://doi.org/10.1093/emboj/17.13.3619.
Werner, P., et al., 2001. Multiple sclerosis: altered glutamate homeostasis in lesions correlates with oligodendrocyte and axonal damage. Ann. Neurol. 50, 169–180. https://doi.org/10.1002/ana.1077.
Xu, J., et al., 2007. Peroxisome proliferator-activated receptor-alpha agonist fenofibrate regulates IL-12 family cytokine expression in the CNS: relevance to multiple sclerosis. J. Neurochem. 103, 1801–1810. https://doi.org/10.1111/j.1471-4159.2007.04875.x.
Yu, G., et al., 2012. clusterProfiler: an R package for comparing biological themes among gene clusters. OMICS. 16, 284–287. https://doi.org/10.1089/omi.2011.0118.
Zhang, Z., et al., 2011. Hypoxia inducible factor-1 as a target for neurodegenerative diseases. Curr. Med. Chem. 18, 4335–4343. https://doi.org/10.2174/092986711797200426.
Zhao, X., et al., 2006. Peroxisome-proliferator-activated receptor-gamma (PPARgamma) activation protects neurons from NMDA excitotoxicity. Brain Res. 1073–1074, 460–469. https://doi.org/10.1016/j.brainres.2005.12.061.